Article

Analysis of TiH$_x$O$_y$ Films Produced by Physical Vapor Deposition Method

Marius Urbonavicius [1,*], Simona Tuckute [1], Smagul Karazhanov [2] and Martynas Lelis [1,*]

1 Lithuanian Energy Institute, Breslaujos st. 3, LT-44403 Kaunas, Lithuania
2 Institute for Energy Technology, P.O. Box 40, NO-2027 Kjeller, Norway
* Correspondence: marius.urbonavicius@lei.lt (M.U.); martynas.lelis@lei.lt (M.L.); Tel.: +370-374-018-24 (M.U.); +370-374-019-04 (M.L.)

Abstract: For decades, partially oxidized hydrides were commonly considered as undesirably contaminated phases and were avoided by scientists. Nevertheless, more recently, it was realized that in some hydrides and oxides, partial substitution of dissimilar H$^-$ and O^{2-} anions allows one to obtain unique optical and electrical properties that might have appealing applications in commercial products. It was determined that specific properties of so called oxyhydride materials strongly depend on the used synthesis methods; therefore, there is a great interest in exploring various variants of oxyhydride formation. In the current study, TiH$_x$O$_y$ films were deposited by a reactive magnetron sputtering process in Ar-O$_2$-H$_2$ gas mixtures. Color, transparency and crystal phase composition of the films coherently reacted to the Ar:O$_2$:H$_2$ gas ratio. Namely, the rise in partial hydrogen pressure promoted the formation of anatase phase TiO$_2$ structure and darkening of the films. Interestingly, this had only minimal impact on the band gap values, but had a relatively strong negative effect on the photocatalytic activity of the films. The unaccustomed results stressed the difference between the partially reduced TiO$_2$ with a significant amount of oxygen vacancies and synthesized TiH$_x$O$_y$ films where some O^{2-} ions are implicitly substituted by H$^-$ ions.

1. Introduction

Oxides, hydrides and hydroxides are common material classes that have been known and used for ages. Oxyhydrides, on the other hand, make up a less known class of multianion materials where the oxide and hydride anions are sharing the same sites within the crystal lattice [1]. The first report on oxyhydride synthesis (namely LaH$_{1+2x}$O$_{1-x}$ and LaH$_{1+y}$O$_{1-x}$ (y < 2x) oxyhydrides) was published 40 years ago [2] and dealt with relatively high skepticism. At that time, researchers assumed that under normal conditions, the coexistence of dissimilarly charged hard O^{2-} anions and soft, polarizable, H$^-$ anions at the same sites of a crystalline solid was thermodynamically unlikely [3,4]. Direct experimental confirmation of hydrogen entering into the oxide structure was and still remains a challenging task, because most of the traditionally used material analysis methods such as X-ray diffraction, energy dispersive spectroscopy, X-ray photoelectron spectroscopy and others can not observe hydrogen directly. Nevertheless, credible crystal structure study by combining neutron and X-ray diffraction techniques [5] unambiguously confirmed the unusual type of oxygen and hydrogen anion site sharing and the existence of oxyhydrides was eventually accepted by the whole scientific community. Many of these materials were obtained by partially oxidizing hydrides and, based on their crystal structure, could be described as oxygen-containing hydrides [6]. However, hydrogen-containing oxides were reported as well [4]. More recently, some authors suggested adopting the usage of the -HO ending for the oxyhydrides [7], thus discriminating them from the hydroxides (i.e., materials with -OH groups).

Following the first reports of LaHO synthesis by J.F. Brice et al. [2,5], some more oxyhydrides were synthesized and identified as well [8–10]. However, in general, the reports of oxyhydride studies remained scarce, and for years these materials had no practical applications. Approximately one decade ago, researchers started to realize that unique properties of hydrogen can lead to the advanced functionality of oxyhydride materials, and the situation started to change drastically [3]. The ionic radius of hydrogen anion (139.9 pm) is relatively similar to the ionic radius of oxygen anion (145.2 pm) [11]; however, at the same time, H^- ion has two times smaller charge and is distinctly easier to polarize than the O^{2-} ion [4]. Accordingly, it was assumed that if O^{2-} were replaced by H^- (or vice versa), this would not induce large disturbances to the crystal lattice, but could create uncommon electron energy level structures and could lead to interesting magnetic and optical properties [3,4,12]. This, in turn, potentially might have appealing applications in commercial products.

Recently, it was reported that in some of the oxyhydrides, H^- and O^{2-} ions might have the possibility of interacting via valence charge states of the metal center [1]. In partially oxidized yttrium hydride and several other rare-earth (Gd, Dy, and Er) hydrides, reversible switching of optical transmittance under intense irradiation was observed [13]. This feature of yttrium oxyhydride is currently being tested for application in smart window devices [14].

Titanium is also recognized for its potential to form corresponding oxyhydride phases [15]. However, up to now, most of the efforts to alter the TiO_2 structure by hydrogen (both in powder and film form) have been focused on the reduction of TiO_2 and the formation of oxygen vacancies that are beneficial for photocatalytic applications. Meanwhile, direct synthesis of ternary titanium oxyhydrides from the constituting elements (namely, titanium oxygen and hydrogen) have not yet been reported, and the practical value of such oxyhydrides has not yet been determined. Accordingly, in the current study, we focused on the controllable one-step synthesis of titanium oxyhydride films by a reactive magnetron sputtering technique. Structural, optical and photocatalytic properties of the as-deposited films were thoroughly analyzed and compared with the corresponding properties of black TiO_2 films and powders, which were prepared by ex situ reduction of TiO_2 (by interaction with hydrogen and other compounds).

2. Materials and Methods

TiHO samples were deposited using a custom modified Kurt J. Lesker PVD-75 physical vapor deposition system equipped with cryo pump and one unbalanced Torrus 3 magnetron. The magnetron had a titanium target (76 mm diameter, 6 mm thickness, 99.99% purity) and was powered by a 300 W DC power source. Ar, O_2 and H_2 gases (all 99.999% purity) were supplied by three mass flow controllers that were operated by a Nova Fabrica FloTron X multi-channel process control system. Three different Ar-O_2-H_2 gas mixtures were used to deposit titanium oxyhydride films with varying hydrogen concentrations. The hydrogen concentration was increased, going from sample B1 to sample B3 (more details are provided in Table 1). In addition, an Ar-O_2 gas mixture was used to deposit conventional titanium dioxide films (samples A). For the deposition of later samples, the same experimental set-up was used. The only modifications to the process were the annulment of hydrogen gas supply and introduction of a pulsed direct-current (p-DC) power source. In the Ar-O_2 gas mixture, the p-DC power source allowed us to prevent titanium target charging/poisoning and improved reactive magnetron sputtering process stability (in the Ar-O_2-H_2 gas mixture, the Ti target was continuously reduced by hydrogen; therefore, for TiHO deposition, the p-DC power source was not needed). Deposition time for all group B samples was the same—1 h, but their deposition rate varied significantly depending on the working gas mixture composition. Accordingly, the ultimate thickness of group B samples reached approximately 700 nm for B1, 900 nm for B2 and 1500 nm for B3. Group A samples were deposited for 2 h, and their thickness was approximately 1500 nm.

Table 1. Main parameters of reactive magnetron sputtering deposition process.

Samples	Ar Flux	O$_2$ Flux	H$_2$ Flux	Ar:O$_2$:H$_2$ Flux Ratio	Total Pressure	Power Source
A	4.5 sccm	1.2 sccm	-	3.78:1:-	6×10^{-3} mbar	300 W p-DC
B1	2.7 sccm	6.4 sccm	15.1 sccm	0.42:1:2.36	6×10^{-3} mbar	300 W DC
B2	2.8 sccm	4.2 sccm	20.1 sccm	0.67:1:4.78	6×10^{-3} mbar	300 W DC
B3	2.8 sccm	3.6 sccm	22.5 sccm	0.78:1:6.25	6×10^{-3} mbar	300 W DC

Crystal structures of the deposited films were determined by X-ray diffraction (XRD, Bruker D8). Elemental composition and chemical states of the TiHO films were analyzed by X-ray photoelectron spectroscopy (XPS, PHI 5000 Versaprobe). To minimize the extent of additional sample surface oxidation and contamination by adventitious hydrocarbons, XPS analysis was carried out straight after the samples were transferred from the deposition chamber to the XPS instrument. Optical transmission and reflectance of the films were acquired by UV–VIS spectrophotometer. To estimate band gap energies of the samples, corresponding Tauc plots were drawn. Since it was not easy to split the Kubelka–Munk spectrum into spectra of individual components (in this case, films and their substrates), a simplified band gap estimation method described in [16] was applied. By this method, at first, the traditional linear part of the plot was extrapolated to the *x*-axis, and an additional linear fit was applied for the slope below the fundamental absorption. Then, a band gap value was determined at the intersection of the corresponding two linear fittings. Photocatalytic activity of TiO$_2$ and TiHO samples was estimated using methylene blue (MB) bleaching test (adopted version of ISO 10678:2010 standard [17]). For these tests, the MB solution volume was 15 mL, and initial concentration 15 mg/L. Photocatalysis was initiated with collimated 365 nm LED light source (Thorlabs M365LP1-C1).

3. Results

Reactive magnetron sputtering under Ar-O$_2$ atmosphere produced a colorless transparent film (sample A) consisting of anatase and rutile TiO$_2$ phases (Figure 1). When the gas mixture was supplemented with hydrogen, the crystallinity of the samples started to weaken, and they started to gain a noticeable tint. At the largest hydrogen concentration (sample B3), the effect was especially strong: the sample nearly lost the rutile phase and obtained a dark blue-grey shade. Traditionally, the appearance of blueish shade in titanium oxide samples is associated with Ti^{4+} reduction to Ti^{3+} and observation of Ti$_2$O$_3$ phase [18,19]. However, during close inspection of TiHO XRD patterns (Figure 1), we did not detect any features that could be attributed to Ti$_2$O$_3$ or any other titanium suboxides.
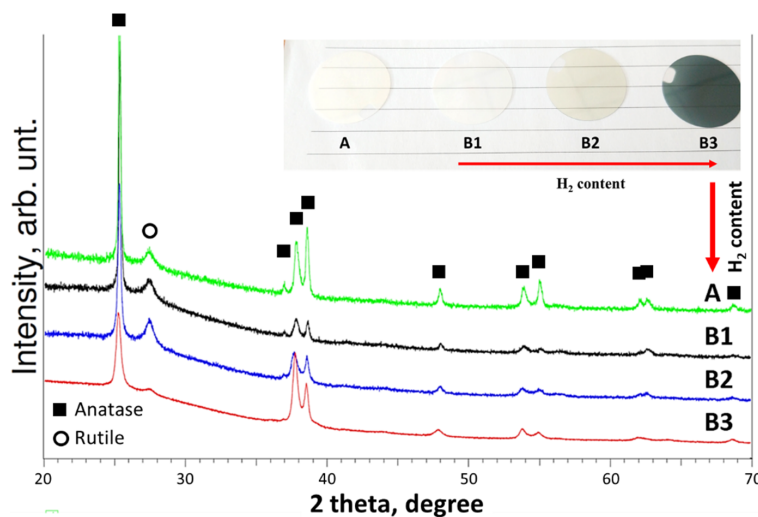
Figure 1. Visual appearance (insert) and XRD patterns of TiO$_2$ (**A**) and TiHO (**B1**–**B3**) samples.

These results are interesting from several perspectives. First, earlier reports demonstrated that Ti-O-H interaction during TiH_2 powder oxidation experiments nearly exclusively results in direct or indirect (i.e., through the intermediate phases of titanium suboxides) formation of the rutile TiO_2 [10,15,20]. Naturally, the processes of TiH_2 oxidation and titanium sputtering in a reactive $Ar-O_2-H_2$ atmosphere have fundamental differences and can not be compared directly. Still, the observed decline in the crystallinity of the thermodynamically most stable rutile TiO_2 phase is not a trivial outcome and supports the indications by other groups [21,22], who suggested that products of Ti-O-H interaction can be method-specific.

Second, in defected TiO_2 samples (including some "black TiO_2" samples produced using hydrogen [23]) the dark color is commonly attributed to the presence of oxygen vacancies and Ti^{3+} species [24–26]. For example, a similar trend of TiO_2 darkening and rutile phase depreciation from the initial anatase-rutile mixture was observed when standard white TiO_2 powders were reduced by $NaBH_4$ [27]. In that study, XPS analysis of reduced TiO_2 powders confirmed that color and structural changes of the initial TiO_2 powders can be attributed to the propagation of oxygen vacancies (indicated by the decrease in bulk O:Ti ratio) and partial reduction of Ti^{4+} to Ti^{3+} state (indicated by the appearance of the additional Ti $2p_{3/2}$ peak component at approximately 457.1 eV).

In order to resolve the discrepancy between the supposed (by the color) and observed crystal structure of TiHO samples, we also used the XPS technique and determined the chemical state of titanium. If it were present, Ti(III) oxide (i.e., Ti^{3+}) should have an O 1s peak component at approximately 532.5 eV and Ti 2p peak components at 457.3 eV and 462.5 eV [28,29]. Moreover, looking at the color changes of the TiHO samples, one might expect that peak components related to Ti(III) oxide should become stronger proceeding from sample B1 to sample B3. Notwithstanding the initial assumptions and significantly different appearance of TiHO samples, all photoelectron spectra of titanium, oxygen and valence-band electrons were nearly identical (Figure 2). More specifically, Ti 2p photoelectron spectra for all TiHO samples had two almost fully symmetrical peaks at approximately 458.7 eV and 464.4 eV. These peaks fit well with the standard Ti $2p_{3/2}$ and Ti $2p_{1/2}$ peak positions of Ti(IV) oxide [28]. Similarly, all acquired O 1s spectra had a strong peak at 530.0 eV with a small shoulder at 531.0–531.5 eV. The main O 1s peak corresponded well with the oxygen from Ti(IV) oxide [28], whereas the higher energy shoulder was attributed to C-O [30] and O-H groups [31] presumably coming from the adventitious surface contamination and moisture.
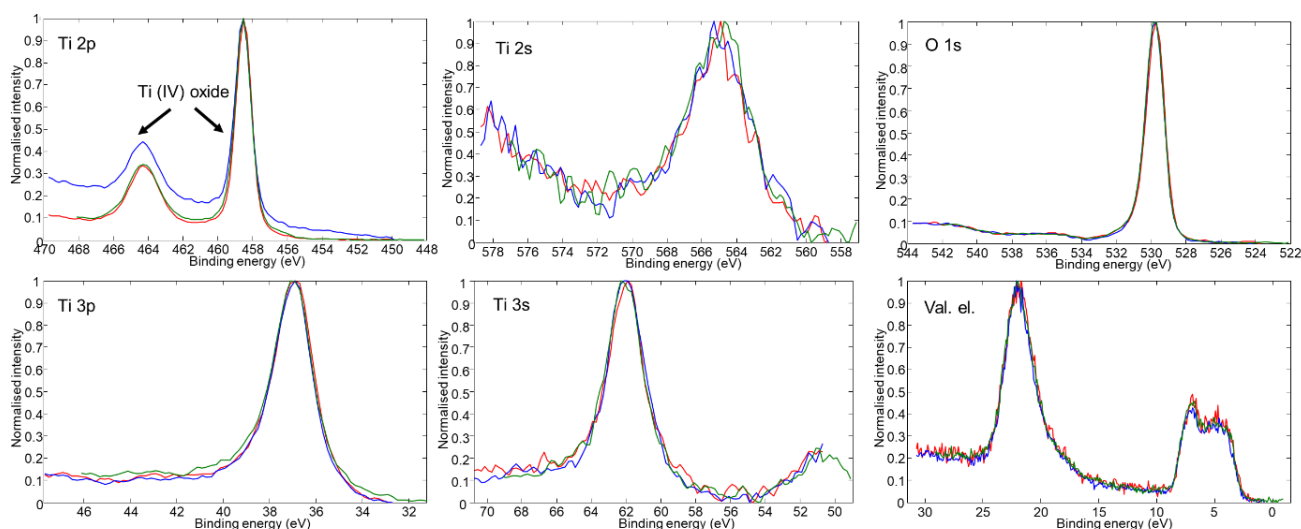

Figure 2. XPS spectra of the as-deposited TiHO films: B1—red, B2—blue, B3—green.

Based solely on the XRD and XPS data, it might be assumed that the only form of titanium in TiHO samples is Ti^{4+} and it makes up only Ti(IV) oxide. But the evident tint of

B2 and B3 samples suggest that this should not be the case. It is likely that other forms of titanium also exist, but they were not detected due to the limitations of the XRD and XPS methods. As mentioned above, the blue tint in Ti-O system traditionally is associated with the presence of Ti^{3+} [18,19]. Considering the limits of the XRD and XPS methods, it can be concluded that other forms of titanium (presumably Ti^{3+} next to the oxygen vacancies, or amorphous Ti_2O_3 regions at grain boundaries) should be present in the bulk of the film.

In defected TiO_2 and mixed TiO_2-Ti_2O_3 materials, Ti^{3+} cations introduce new electron levels just bellow the conduction band of TiO_2 and result in the strong absorbance (mostly witnessed as a fall in light transmittance) above 500–600 nm [19,21,32]. At the same time, these materials demonstrate an increase in reflectance starting from 400–600 nm (the position of the lower end of reflectance increase depends on the oxygen content [21]). In order to test if as-deposited TiHO films have these optical characteristics of Ti^{3+} oxides, optical transmittance and reflectance measurements were performed (Figure 3). Typically for standard TiO_2 films, above 400 nm, sample A had a stable transmittance level of nearly 80% and reflectance of approximately 20%. Films deposited with low and medium hydrogen concentrations (samples B1 and B2) had slightly lower optical transmittance, but it remained relatively stable over the whole tested range. Sample B3, on the other hand, had a considerably lower transmittance, which peaked out at 500 nm and reached just over 30%. Such transmittance spectra are typical for Ti(III) oxide [22], but there was no rise in reflectance spectra, and this feature distinguished the B3 samples from other reported blue tinted defected TiO_2 and/or Ti_2O_3 films [4,21].
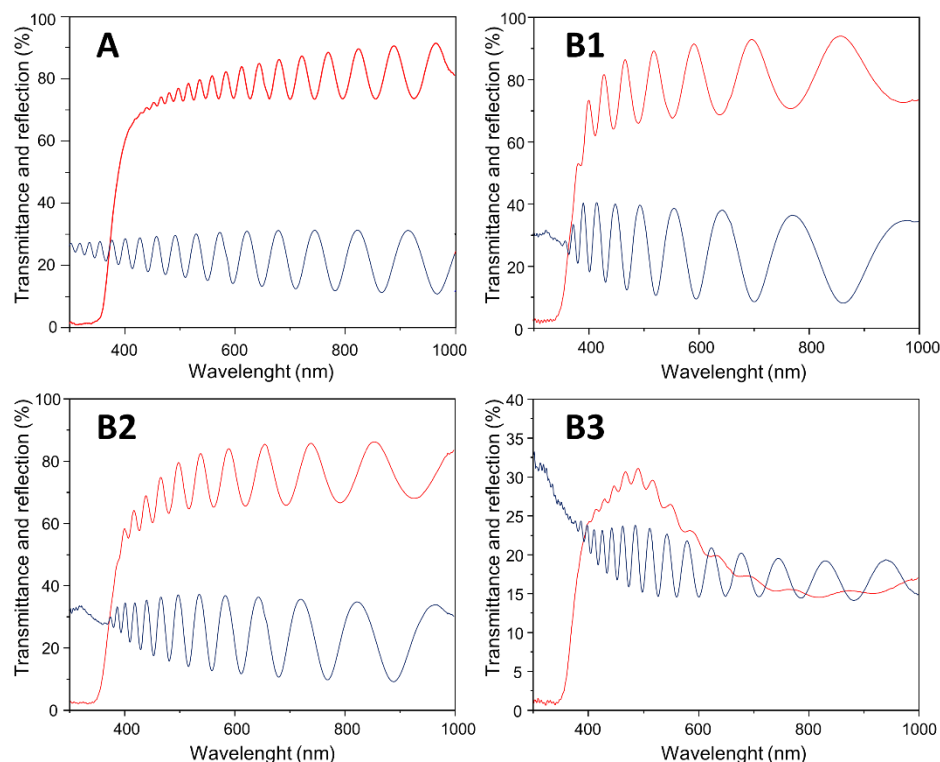

Figure 3. Optical transmittance (**red**) and reflection (**blue**) of TiHO films.

Another interesting characteristic of the current TiHO films is that higher hydrogen content resulted in slightly higher optical band gap values (samples B1 and B3 had band gap values of 3.25 and 3.26 eV, respectively, Figure 4) than that of standard TiO_2 (sample A had a band gap of 3.22 eV). Meanwhile, the reported band gap values of reduced or defected TiO_2 materials had a tendency to be lower [4]. Additionally, as a common trend, reduced or defected TiO_2 oxides have higher photocatalytic activity [27]. However, in the current study, photocatalytic MB bleaching efficiency using tinted TiHO films (samples B2

and B3) was weaker in comparison to that with samples A and B1, which were deposited using lower hydrogen fractions in the gas mixture (Figure 5).
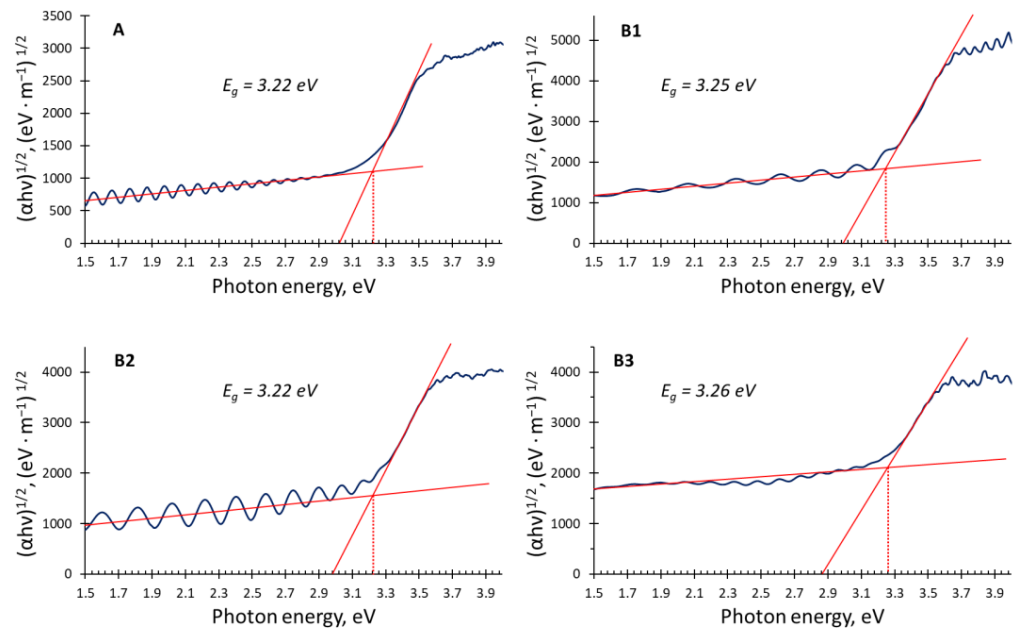

Figure 4. Tauc plots (blue curves), trendlines for the linear parts of the plots (solid red lines) and respective band gap values (dotted red lines) of TiHO films.
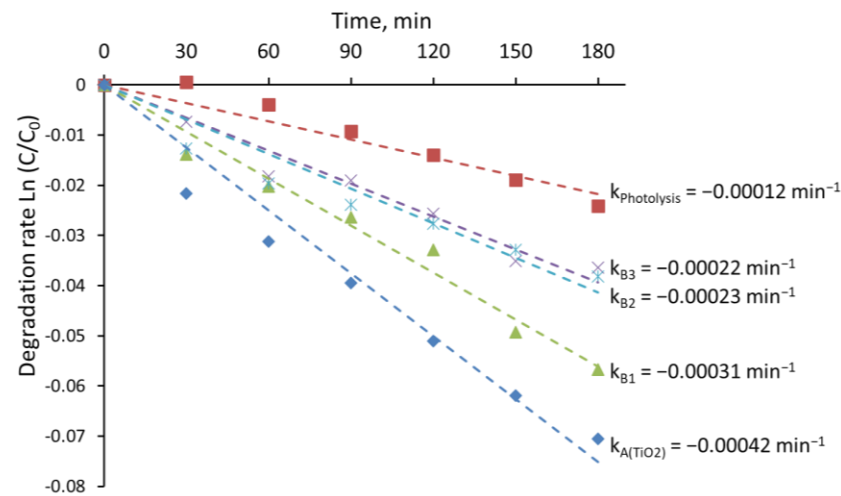

Figure 5. Estimation of photocatalytic bleaching of MB solution using different TiHO films.

4. Discussion

Summing up the observed results, it can be concluded that reactive magnetron sputtering of titanium in Ar-O_2-H_2 gas mixtures with high hydrogen content allows the deposition of films whose visual appearance is similar to the titanium oxide with a significant amount of titanium in Ti^{3+} state. However, neither of the applied methods provided unambiguous evidence for the existence of Ti(III) oxide or oxygen vacancies. This suggests that during film deposition, hydrogen not only reduces TiO_2 and stimulates the formation of oxygen vacancies, but also presumably creates bonds with titanium and occupies oxygen sites in crystal structures of Ti(IV) oxides. Earlier studies with various oxyhydrides [4] demonstrated that when hydrogen occupies oxygen sites, it can stabilize the crystal structure of the corresponding oxide and extend its stability to lower oxygen contents [4,21]. We assume that in currently investigated TiHO samples, hydrogen also stabilized the Ti(IV)

crystal structure and averted the nucleation growth of crystalline Ti_2O_3 or other titanium suboxide phases.

The absence of Ti^{3+} component in XPS spectra also might be related to the fact that in TiHO samples, instead of oxygen vacancies, there are highly polarizable H^- anions. These anions can hinder the Ti^{3+} signal in two ways. First, although hydrogen has a lower charge than oxygen, it is still higher than the efficient charge of oxygen vacancy. Second, there is high thermodynamic potential for the hydrogen anions to combine and form neutral hydrogen molecules. Indeed, recently, researchers demonstrated that full oxidation of some oxyhydrides is even easier to achieve than oxidation of corresponding suboxides [4]. This means that in oxyhydride materials, the chemical bonds of hydrogen with the cations is not strong, and hydrogen might be relatively easily replaced by oxygen from the atmosphere. Accordingly, there is a probability that during TiHO sample transfer from the deposition chamber to XPS, hydrogen from the top layers of the TiHO samples was rapidly replaced by oxygen from the atmosphere, and after this oxidation, only Ti^{4+} peaks were acquired. Similar reasoning also can be used to explain the unexpectedly low photocatalytic activity of TiHO films. First, due to the relatively high reactivity of hydrogen in oxyhydrides, by placing TiHO samples into aqueous solutions, we might initiate additional TiHO sample oxidation by hydrolysis. This potentially may eliminate the beneficial Ti^{3+} cations from the sample and reduce the induction of electron-hole pairs. On the other hand, if hydrogen is not removed from the oxygen sites, its high polarizability might serve for the higher recombination rates of photoinduced charges.

5. Conclusions

The nature of oxyhydrides and technical challenges in direct observation of hydrogen anions make the identification and characterization of TiHO films complicated. Nevertheless, discrepancies between the structural and optical properties of the deposited films and previously reported Ti_2O_3 and other titanium suboxide materials (including reduced black TiO_2) allow us to assume that reactive magnetron sputtering of titanium in an Ar-O_2-H_2 gas mixture forms TiHO films with the crystal structure of TiO_2. When some O^{2-} anions are replaced by H^- anions and hydrogen sits at oxygen sites, small and easily polarizable H^- ions stabilize the oxide crystal structure and halt the nucleation and/or growth of the Ti_2O_3 crystal phase. XPS analysis revealed that despite the different tints of TiHO films at the surface, all of them were composed almost solely of Ti(IV) oxide. The main reason for such composition may be related to the potentially high reactivity of hydrogen anions, which easily react with atmospheric oxygen. In order to test the provided assumptions, additional Raman spectroscopy and glow discharge optical emission spectroscopy measurements are planned to be taken in the future.

Author Contributions: Conceptualization and methodology: M.L.; experimental testing and validation M.U., M.L., S.K. and S.T.; analysis of the results and preparation of draft paper, M.L.; revision and edition, M.L., M.U., S.K. and S.T. All authors have read and agreed to the published version of the manuscript.

Institutional Review Board Statement: Not applicable.

Informed Consent Statement: Not applicable.

Data Availability Statement: Not applicable.

Conflicts of Interest: The authors declare no conflict of interest.

References

1. Pishtshev, A.; Strugovshchikov, E.; Karazhanov, S. Conceptual Design of Yttrium Oxyhydrides: Phase Diagram, Structure, and Properties. *Cryst. Growth Des.* **2019**, *19*, 2574–2582. [CrossRef]
2. Brice, J.F.; Moreau, A. Synthèse et conductivité anionique des hydruro-oxydes de lanthane de formule LaHO, $LaH_{1+2x}O_{1-x}$ et $LaH_{1+y}O_{1-x}$ (y < 2x). *Ann. Chim.* **1982**, *7*, 623–634.
3. Norby, T.; Widerøe, M.; Glöckner, R.; Larring, Y. Hydrogen in oxides. *Dalton Trans.* **2004**, *19*, 3012–3018. [CrossRef] [PubMed]
4. Kobayashi, Y.; Hernandez, O.; Tassel, C.; Kageyama, H. New chemistry of transition metal oxyhydrides. *Sci. Technol. Adv. Mater.* **2017**, *18*, 905–918. [CrossRef] [PubMed]
5. Malaman, B.; Brice, J.F. Etude structurale de l'hydruro-oxyde LaHO par diffraction des rayons X et par diffraction des neutrons. *J. Solid State Chem.* **1984**, *53*, 44–54. [CrossRef]
6. Montero, J.; Martinsen, F.A.; Lelis, M.; Karazhanov, S.Z.; Hauback, B.C.; Marstein, E.S. Preparation of yttrium hydride-based photochromic films by reactive magnetron sputtering. *Sol. Energy Mater. Sol. Cells* **2018**, *177*, 106–109. [CrossRef]
7. Moldarev, D.; Moro, M.V.; You, C.C.; Baba, E.M.; Karazhanov, S.Z.; Wolff, M.; Primetzhofer, D. Yttrium oxyhydrides for photochromic applications: Correlating composition and optical response. *Phys. Rev. Mater.* **2018**, *2*, 115203. [CrossRef]
8. Rotella, F.J.; Flotow, H.E.; Gruen, D.M.; Jorgensen, J.D. Deuterium site occupation in the oxygen-stabilized η-carbides $Zr_3V_3OD_x$. I. Preparation and neutron powder diffraction. *J. Chem. Phys.* **1983**, *79*, 4522–4531. [CrossRef]
9. Clark, N.J.; Wu, E. Hydrogen absorption by M_5X_3 phase Zr-Al compounds. *J. Less Common Met.* **1988**, *142*, 145–154. [CrossRef]
10. Lavrenko, V.A.; Shemet, V.Z.; Petrov, L.A.; Teplov, O.A.; Dolukhanyan, S.K. High-temperature oxidation of titanium-hydride powders. *Oxid. Met.* **1990**, *33*, 177–189. [CrossRef]
11. Lang, P.F.; Smith, B.C. Ionic radii for Group 1 and Group 2 halide, hydride, fluoride, oxide, sulfide, selenide and telluride crystals. *Dalton Trans.* **2010**, *39*, 7786–7791. [CrossRef] [PubMed]
12. You, C.C.; Mongstad, T.; Maehlen, J.P.; Karazhanov, S. Engineering of the band gap and optical properties of thin films of yttrium hydride. *Appl. Phys. Lett.* **2014**, *105*, 31910. [CrossRef]
13. Baba, E.M.; Montero, J.; Moldarev, D.; Moro, M.V.; Wolff, M.; Primetzhofer, D.; Sartori, S.; Zayim, E.; Karazhanov, S. Preferential Orientation of Photochromic Gadolinium Oxyhydride Films. *Molecules* **2020**, *25*, 3181. [CrossRef] [PubMed]
14. Strugovshchikov, E.; Pishtshev, A.; Karazhanov, S. Theoretical Design of Effective Multilayer Optical Coatings Using Oxyhydride Thin Films. *Phys. Status Solidi* **2021**, *258*, 2100179. [CrossRef]
15. Fokin, V.N.; Malov, Y.I.; Fokina, E.E.; Troitskaya, S.L.; Shilkin, S.P. Investigation of interactions in the TiH_2-O_2 system. *Int. J. Hydrogen Energy* **1995**, *20*, 387–389. [CrossRef]
16. Makuła, P.; Pacia, M.; Macyk, W. How To Correctly Determine the Band Gap Energy of Modified Semiconductor Photocatalysts Based on UV–Vis Spectra. *J. Phys. Chem. Lett.* **2018**, *9*, 6814–6817. [CrossRef] [PubMed]
17. *ISO 10678:2010*; Fine Ceramics (Advanced Ceramics, Advanced Technical Ceramics)—Determination of Photocatalytic Activity of Surfaces in an Aqueous Medium by Degradation of Methylene Blue. International Organization for Standardization: Geneva, Switzerland, 2010.
18. Diebold, U. The surface science of titanium dioxide. *Surf. Sci. Rep.* **2003**, *48*, 53–229. [CrossRef]
19. Cronemeyer, D.C. Infrared Absorption of Reduced Rutile TiO_2 Single Crystals. *Phys. Rev.* **1959**, *113*, 1222–1226. [CrossRef]
20. Kennedy, A.R.; Lopez, V.H. The decomposition behavior of as-received and oxidized TiH_2 foaming-agent powder. *Mater. Sci. Eng. A* **2003**, *357*, 258–263. [CrossRef]
21. Barros, H.W.S.; Duarte, D.A.; Sagás, J.C. Optical and electrical properties of Ti suboxides grown by reactive grid-assisted magnetron sputtering. *Thin Solid Film.* **2020**, *696*, 137762. [CrossRef]
22. Stryhalski, J.; Duarte, D.A.; Rebouta, L.M.; Sagas, J.C.; Tavares, C.J.; Fontana, L.C. Nb-doped Ti_2O_3 Films Deposited through Grid-Assisted Magnetron Sputtering on Glass Substrate: Electrical and Optical Analysis. *Mater. Res.* **2019**, *22*, e20180524. [CrossRef]
23. Godoy Junior, A.; Pereira, A.; Gomes, M.; Fraga, M.; Pessoa, R.; Leite, D.; Petraconi, G.; Nogueira, A.; Wender, H.; Miyakawa, W.; et al. Black TiO_2 Thin Films Production Using Hollow Cathode Hydrogen Plasma Treatment: Synthesis, Material Characteristics and Photocatalytic Activity. *Catalysts* **2020**, *10*, 282. [CrossRef]
24. Xiu, Z.; Guo, M.; Zhao, T.; Pan, K.; Xing, Z.; Li, Z.; Zhou, W. Recent advances in Ti^{3+} self-doped nanostructured TiO_2 visible light photocatalysts for environmental and energy applications. *Chem. Eng. J.* **2020**, *382*, 123011. [CrossRef]
25. Di Valentin, C.; Pacchioni, G.; Selloni, A. Reduced and n-type doped TiO_2: Nature of Ti^{3+} species. *J. Phys. Chem. C* **2009**, *113*, 20543–20552. [CrossRef]
26. Sarkar, A.; Khan, G.G. The formation and detection techniques of oxygen vacancies in titanium oxide-based nanostructures. *Nanoscale* **2019**, *11*, 3414–3444. [CrossRef]
27. Andronic, L.; Lelis, M.; Enesca, A.; Karazhanov, S. Photocatalytic activity of defective black-titanium oxide photocatalysts towards pesticide degradation under UV/VIS irradiation. *Surf. Interfaces* **2022**, *32*, 102123. [CrossRef]
28. Naumkin, A.V.; Kraut-Vass, A.; Gaarenstroom, S.W.; Powell, C.J. *NIST X-Ray Photoelectron Spectroscopy Database, NIST Standard Reference Database 20*; Version 4.1; On-Line Database, Updated on 2012; NIST: Gaithersburg, MD, USA, 2012.
29. An, H.-R.; Park, S.Y.; Kim, H.; Lee, C.Y.; Choi, S.; Lee, S.C.; Seo, S.; Park, E.C.; Oh, Y.-K.; Song, C.-G.; et al. Advanced nanoporous TiO_2 photocatalysts by hydrogen plasma for efficient solar-light photocatalytic application. *Sci. Rep.* **2016**, *6*, 29683. [CrossRef]

30. Liu, H.; Liu, S.; Zhang, Z.; Dong, X.; Liu, T. Hydrothermal etching fabrication of TiO$_2$@graphene hollow structures: Mutually independent exposed {001} and {101} facets nanocrystals and its synergistic photocaltalytic effects. *Sci. Rep.* **2016**, *6*, 33839. [CrossRef]

31. Krishnan, P.; Liu, M.; Itty, P.A.; Liu, Z.; Rheinheimer, V.; Zhang, M.-H.; Monteiro, P.J.M.; Yu, L.E. Characterization of photocatalytic TiO$_2$ powder under varied environments using near ambient pressure X-ray photoelectron spectroscopy. *Sci. Rep.* **2017**, *7*, 43298. [CrossRef]

32. Ghosh, A.K.; Wakim, F.G.; Addiss, R.R. Photoelectronic Processes in Rutile. *Phys. Rev.* **1969**, *184*, 979–988. [CrossRef]